The activation of hematite for the catalytic hydrogen peroxide degradation of Methylene Blue

Fangju Huang, Haibo Liu*, Hanlin Wang, Fuwei Sun, Tianhu Chen, Dong Chen, Qiaoqin Xie, Yuefei Zhou, Yueling Zhao

[a]Key Laboratory of Nano-minerals and Pollution Control of Anhui Higher Education Institutes, Hefei University of Technology, Hefei 230009, China, Tel. +8615856995526; emails: liuhaibosky116@hfut.edu.cn (H. Liu), 1359261791@qq.com (F. Huang), hanlinwang@mail.hfut.edu.cn (H. Wang), 1019285549@qq.com (F. Sun), chentianhu@hfut.edu.cn (T. Chen), cdxman@hfut.edu.cn (D. Chen), qqxie424@hfut.edu.cn (Q. Xie), alphazhou@hfut.edu.cn (Y. Zhou), 1123744762@qq.com (Y. Zhao)
[b]Environmental Mineral and Material, School of Resources and Environmental Engineering, Hefei University of Technology, Hefei 230009, China

ABSTRACT

The activation of hematite was conducted via thermal treatment in a hydrogen atmosphere to form zero-valent iron (ZVI). The physicochemical properties of ZVI before and after reaction were characterized via X-ray diffraction and X-ray photoelectron spectroscopy. The effects of ZVI dose, H_2O_2 concentration, initial pH, reaction temperature, initial MB concentration, and different anions on the degradation of MB were examined. The degradation mechanism was elucidated by combining the analysis of total organic carbon (TOC) removal, electron paramagnetic resonance, and UV-Vis. When the ZVI dose is 69 mg/L with an initial pH of 3.0, approximately 100% of color was removed, and a 47% TOC degradation was achieved. Furthermore, after ZVI was cycled seven times, the decolorization efficiency had only a slight decrease, which implies an excellent stability. Fe^{2+} released by ZVI is important and was essential in the catalytic H_2O_2 degradation of MB. The experimental data showed that H_2O_2 was catalyzed by activated hematite in the Fenton process. This observation indicated that the activation of hematite to prepare ZVI was a promising method and had a considerable application value and potential for the MB degradation.

Keywords: Hematite; Activation; Heterogeneous catalysis; Methylene blue; Mechanism

1. Introduction

As well know, advanced oxidation processes (AOPs) [1,2] (e.g., Fenton, photolysis, and ozonation) are widely used in wastewater treatment. Organic pollutants are oxidized using the abovementioned methods to harmless products with high biodegradability and low chemical stability [3,4]. The Fenton process is a potential method to treat dye wastewater due to the generation of hydroxyl radicals that can degrade non-biodegradable organic pollutants.

Methylene blue (MB), which is an extensively used and toxic dye, can result in hemolysis, skin irritation, nausea, vomiting, and respiratory distress [5,6]. Thus, MB is chosen to be the target pollutant. However, a conventional homogeneous Fenton process has some restrictions due to its drawbacks including narrow pH range (pH 2.0–3.0), the need to neutralize the solution after the treatment, and the generation of iron-containing sludge [7–9]. Thus, a heterogeneous Fenton process was proposed to solve these common problems of the traditional homogeneous Fenton

* Corresponding author.

process. Recently, a heterogeneous Fenton process, which is based on Fe-bearing materials [e.g., zero-valent iron (ZVI) [10–12], magnetite [13], siderite [8,14], and goethite [15], has received considerable attention. The heterogeneous Fenton reaction system retains the reaction rate and non-selective oxidation of a classical Fenton reaction and also broadens the reaction pH value. Moreover, it is important to develop the heterogeneous Fenton process to reduce the formation of iron sludge and increase recyclability. To our knowledge, ZVI (Fe^0) has been widely used as a well-established catalyst in heterogeneous Fenton processes to eliminate various organic and inorganic pollutants (e.g., chlorinated solvents [16], polychlorinated biphenyls [17,18], dye effluents [19], and heavy metals [20]) from the environment due to its large specific surface area [21], strong surface activity and low cost. Donadelli et al. [22] used ZVI to catalyze H$_2$O$_2$ to degrade azo-dye Acid Black 1 in dye wastewater. Chang et al. [11] reported that ZVI coupled with UV/H$_2$O$_2$ processes effectively decolorized Acid Black 24 wastewater. Ertugay and Acar [12] determined that a 100% decolorization of Direct Blue 71 was obtained using ultrasound/ZVI/H$_2$O$_2$. There are many effective methods for producing ZVI such as hydroboron-palladium acetate [16,23], bimetallic core/shell Fe/Ni nanoparticles [19], and sodium borohydride reduction [20]. In addition, hydrogen reduction is an efficient method to prepare ZVI, which possesses high purity, great magnetic performance, and excellent stability [24,25]. In this study, to lower the preparation cost and promote the comprehensive utilization of natural minerals, oolitic hematite was selected as the source to prepare ZVI.

Oolitic hematite is a mineral resource with porous structure and high chemical reactivity [26]; oolitic hematite accounts for 9% of the total iron ore reserves in China [27]. Many studies have reported the use of hematite for the removal of heavy metal ions or dye wastewater by adsorption and redox reactions [28–31]. However, little attention has been focused on the Fenton process. Therefore, in this study, the activation of the oolitic hematite catalyst was carried out to prepare ZVI to catalyze the H$_2$O$_2$ degradation of MB. The study objectives are to (1) activate oolitic hematite by hydrogen to obtain ZVI, (2) investigate the effects of various conditions (e.g., ZVI dose, H$_2$O$_2$ concentration, initial pH, reaction temperature, initial MB concentration, and different anions) on the degradation efficiency, and (3) illustrate the degradation mechanism, stability, and reusability.

2. Experimental

2.1. Materials and reagents

MB (C$_{16}$H$_{18}$ClN$_3$S) was purchased from Tianjin Fuchen Chemical Reagents Factory of China. Hydrogen peroxide (H$_2$O$_2$) (30%), HCl, NaOH, sodium chloride (NaCl), sodium sulfate (Na$_2$SO$_4$), sodium nitrite (NaNO$_2$), sodium nitrate (NaNO$_3$) were of analytic grade and used without any pretreatment. Oolitic hematite [30–32] was obtained from the Heishiban region of Enshi, Hubei Province, China and was mainly composed of hematite, a small amount quartz, illite, and apatite [26] and it's chemical composition contains Fe$_2$O$_3$ 82.90 wt.%, SiO$_2$ 8.20 wt.%, Al$_2$O$_3$ 4.10 wt.%, CaO 1.90 wt.%, P$_2$O$_5$ 1.30 wt.%, MgO 0.70 wt.%, MnO 0.20 wt.%.

2.2. Experimental procedure

In this study, oolitic hematite was used to prepare ZVI by hydrogen reduction. Briefly, 3.0 g of oolitic hematite (<0.075 mm) was placed in a tube furnace and heated to a designated temperature at a rate of 10°C 1/min under H$_2$ at a flow rate of 20 mL/min to obtain ZVI. All experiments were carried out in a 250 mL beaker containing 200 mL MB solution (50–500 mg/L). The pH of MB was adjusted based on the 0.001–1.0 mol/L HCl and NaOH. The degradation reaction was initiated by adding a certain quantity of ZVI and H$_2$O$_2$ using a blender. A total of 8.0 mL of the reaction solution was collected at designed time intervals and filtered using 0.22 μm syringe filters (PES).

2.3. Analytical techniques

The MB concentrations were analyzed by a UV-visible spectrophotometer (VIS-722N) at 665 nm. The MB structure was observed by a UV-vis spectrophotometer (Shimadzu, UV-1750). The X-ray diffraction (XRD) patterns of the oolitic hematite and activated products were recorded by an X-ray diffractometer (D/max-RB, Japanese) with a Cu K_α radiation in the 2θ range of 5°–70° with a step size of 0.02°. The valence states of elements in the samples were determined by X-ray photoelectron spectroscopy (XPS, Thermo ESCALAB250Xi, America). The chemical information was measured by X-ray fluorescence spectrometry (Shimadzu, XRF-1800). The total organic carbon (TOC) of the reaction solution was determined by Mutil N/C 3000. The concentration of Fe^{2+} and Fe^{3+} was measured by the phenanthroline method. The electron paramagnetic resonance (EPR) experiment was carried out to analyze samples using an EPR spectrometer (JES-FA200, JEOL, Japan) with 5,5-dimethyl-1-pyrroline N-oxide (DMPO) as the spin trapping agent.

3. Results and discussion

3.1. XRD and XPS results of ZVI before and after the reaction

Fig. 1a shows the XRD patterns of oolitic hematite and the activated products before and after the reaction. Combined with the standard cards (JCPD77-1060, JCPD12-531, and JCPD86-2368), it can be observed that 2θ = 33.3°, 35.8°, 40.9°, 49.6°, 54.2°, 57.6°, 62.6°, and 64.1° are the reflections of hematite. When the thermal treatment temperature reaches 300°C, the main phase in the thermally treated product is still hematite, while the reflections intensity becomes weak. When the calcination temperature reaches 400°C, the reflections of magnetite appear at 2θ = 35.6°, 43.2°, 57.2°, and 62.8°, while the reflections of hematite almost entirely disappeared (Fig. 1a). When the temperature reaches 500°C, the reflections of ZVI begins to appear at 44.4° and 64.9°, but the peak intensity is weak. With temperature increasing to 600°C, the reflections of ZVI are stronger than those at 500°C, which indicates that a highly crystalline ZVI was successfully prepared. The XRD peaks of ZVI after the reaction were considerably weaker than those before the reaction, which indicates that ZVI was consumed during the reaction.

XPS was used to study the species on the surface of ZVI before and after the reaction. Fig. 1b shows that the

peaks at 706.9, 710.7, and 711.6 eV belong to Fe^0, Fe^{2+}, and Fe^{3+}, respectively [33]. After the reaction, the peak of Fe^0 at 706.9 eV completely disappears, and the peak at 710.7 eV ascribed to Fe^{2+} is considerably reduced; the peak ascribed to Fe^{3+}/TFe simultaneously increases, which indicates that Fe^0 and part of Fe^{2+} were oxidized to Fe^{3+}.

3.2. Effect of ZVI dose and H_2O_2 concentration

As shown in Fig. 2a, when only H_2O_2 (5.0 mM) was present, the decolorization efficiency of MB reached only 25% due to the stable structure of MB. The decolorization efficiency increases with an increase in the ZVI dose and reaches a maximum of nearly 100% in the presence of 69 mg/L ZVI within 60 min, which indicates that the presence of ZVI is essential and induced heterogeneous Fenton reactions [Eqs. (1)–(3)] [34,35]. However, with a further increase in the ZVI dose, the decolorization efficiency of MB decreases, which may be attributed to the excess of Fe species that are formed by ZVI scavenged $HO^\bullet$ via the reaction [Eq. (4)] [36,37]. The effect of H_2O_2 concentration is illustrated in Fig. 2b. Only 9% decolorization efficiency
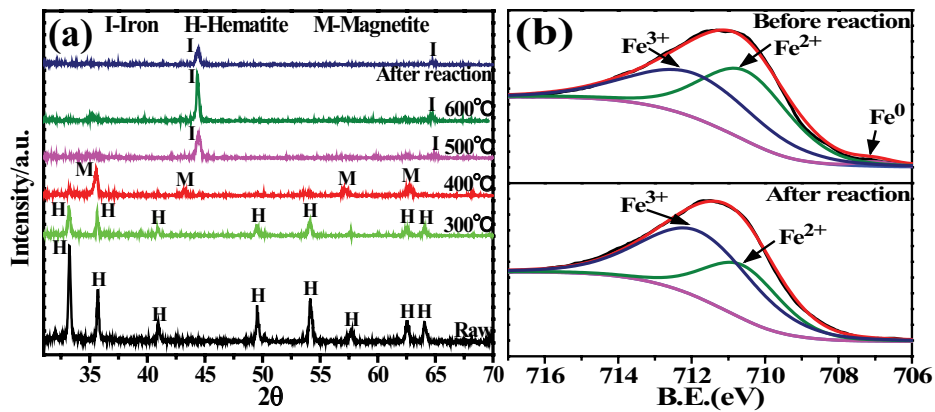
Fig. 1. Characterization of ZVI (a) XRD patterns before and after reaction and (b) XPS spectra before and after reaction.
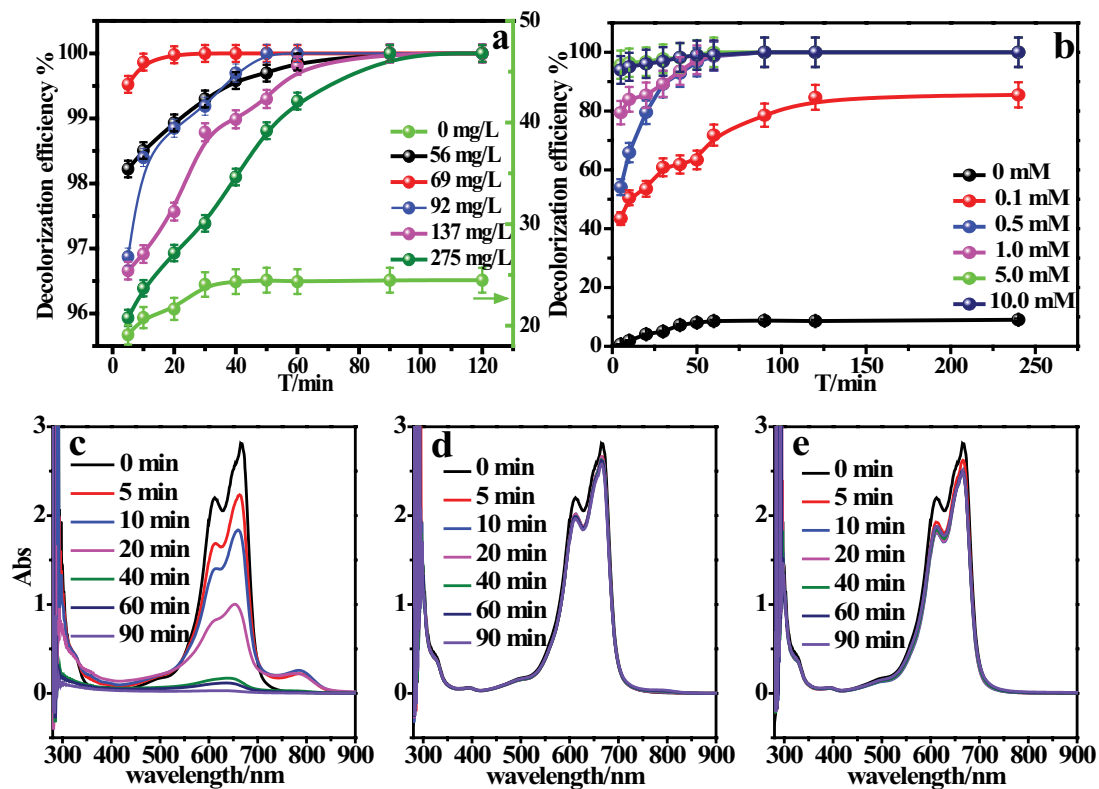
Fig. 2. Effects of (a) ZVI doses (pH = 3.0, C_{MB} = 50 mg/L, $C_{H_2O_2}$ = 5.0 mM, T = 298 K), (b) H_2O_2 concentration (pH = 3.0, C_{MB} = 50 mg/L, ZVI = 69 mg/L, T = 298 K); UV-Vis spectra of the MB solutions (pH = 3.0, C_{MB} = 50 mg/L, T = 298 K), (c) $C_{H_2O_2}$ = 5.0 mM, ZVI = 69 mg/L, (d) ZVI = 69 mg/L, and (e) $C_{H_2O_2}$ = 5.0 mM).

is observed in the presence of only ZVI (69 mg/L), which indicates that the reduction caused by ZVI is small and can be neglected. The decolorization efficiency considerably increased in the presence of H_2O_2, which may be due to the formation of $HO^\bullet$ when ZVI catalyzes H_2O_2. However, with a further increase in the H_2O_2 concentration to 10.0 mM, a slight decrease in the decolorization efficiency was observed. The decrease can be explained by captured $HO^\bullet$ by excess H_2O_2, which leads to the formation of $HO_2^\bullet$ with a lower oxidation ability, as shown in Eqs. (5) and (6) [34,38].

$$Fe^0 + 2H^+ \rightarrow Fe^{2+} + H_2 \tag{1}$$

$$Fe^{2+} + H_2O_2 \rightarrow Fe^{3+} + OH^- + HO^\bullet \tag{2}$$

$$2Fe^{3+} + Fe^0 \rightarrow 3Fe^{2+} \tag{3}$$

$$Fe^{2+} + HO^\bullet \rightarrow Fe^{3+} + OH^- \tag{4}$$

$$H_2O_2 + HO^\bullet \rightarrow H_2O + HO_2^\bullet \tag{5}$$

$$HO_2^\bullet + HO^\bullet \rightarrow H_2O + O_2 \tag{6}$$
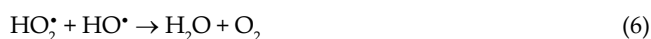
During the degradation process, a variation in the MB solution was recorded by UV-vis spectra at different reaction times, as shown in Figs. 2c–e. The results show one main band of MB with maximum absorption at 665 nm, while the small shoulder at 615 nm was attributed to the absorbance of the dye before degradation [39]. As shown in Fig. 2c, the absorption peak at 665 nm rapidly decreased, and the visible band of MB at 615 nm gradually disappeared, which indicated that a fast degradation of MB can be effectively achieved in the presence of ZVI and H_2O_2. In Figs. 2d and e, the existence of only ZVI or H_2O_2 cause the intensity of the absorption peak at 665 and 615 nm to slightly weaken. Thus, the MB degradation by ZVI or H_2O_2 is not dominant. The results of the experiment are consistent with the abovementioned results.

3.3. Effect of the initial pH

It is known that pH is one of the most important factors during $HO^\bullet$ production in the heterogeneous Fenton process [40,41]. The decolorization efficiency of MB at different initial pH values is shown in Fig. 3a. At pH 3.0, the MB decolorization efficiency is the highest with a 9.48 mg/L/min degradation rate. A further decrease in the pH value to 2.0 results in a poor degradation efficiency than that at pH 3.0. This occurs because excess H^+ can react with $HO^\bullet$ to form water [42], which results in a decline in the MB decolorization efficiency. When the initial pH value varied from 3.0 to 8.0, the decolorization efficiency of the MB sharply decreased from 100% to 19.7% within 90 min. The phenomenon occurs because acidic conditions are beneficial to the promoted generation of $HO^\bullet$ [43]. In addition, the inhibition can be explained by the formation of a hydroxy iron complex and iron hydroxide precipitate and the reaction between OH^- and H_2O_2, which releases O_2 and decreases the $HO^\bullet$ concentration [44,45]. The trend of Fe^{2+}/TFe overtime during the degradation process is shown in

Fig. 3b. It is observed that Fe^{2+}/TFe gradually increased and reaches the maximum value at 1.5 h. After 1.5 h, Fe^{2+}/TFe gradually decreased because Fe^{2+} reacted with H_2O_2 to form large quantities of Fe^{3+}, which increased the Fe^{3+} concentration and decreased the Fe^{2+} concentration. Simultaneously, the Fe^{2+} concentration was significantly higher at pH 3.0 than that at pH 5.0 and 7.0. It is further demonstrated that ZVI was more easily converted to Fe^{2+} under acidic conditions [46], which has a positive role on the dye decolorization by H_2O_2.

3.4. Effect of the initial MB concentration and reaction temperature

In this study, a series of experiments were conducted to explore the effect of the initial MB concentration. As shown in Fig. 3c, the MB decolorization efficiency slightly decreased with an increase in the initial MB concentration from 50 to 500 mg/L. This occurred because the number of MB molecules increased. However, the amount of $HO^\bullet$ was constant, which resulted in the decreasing degradation of MB [42,46].

Fig. 3d shows the effect of reaction temperature on the MB decolorization. An increase in the temperature from 10°C to 25°C considerably enhanced the MB decolorization from 88% to 97% within 20 min. This phenomenon occurs because [8]: (1) high temperature is conducive to the release of Fe^{2+} from ZVI; (2) high temperature increases the formation of $HO^\bullet$, and (3) contributes to the molecular diffusion of radicals. Compared with the decolorization efficiency at 25°C and 40°C, little difference in the MB decolorization was observed.

3.5. Effect of anions

Inorganic anions were usually detected in dye wastewater, and their presence affects the oxidation efficiency of the Fenton process [47–49]. In this section, Cl^-, SO_4^{2-}, NO_2^- and NO_3^- were selected as target anions to investigate the effect of coexisting anions, and the results are shown in Figs. 4a and b. There is little inhibition on the MB decolorization in the presence of Cl^- and SO_4^{2-} at concentrations from 0 to 100 mg/L. With an increase in the concentration to 200 mg/L, inhibition of these anions can be observed over time. These results are observed because (i) both Cl^- and SO_4^{2-} can scavenge $HO^\bullet$ to form other radicals that have a lower oxidation ability and (ii) Fe-anion complexes were generated [48,50]. For the nonspecific adsorption between ZVI and anions (e.g., NO_3^- and NO_2^-), the results are shown in Figs. 4c and d; the inhibitory effect was obvious with an increase in the concentration. This occurs because NO_3^- and NO_2^- can easily react with $HO^\bullet$, which results in a decrease in the $HO^\bullet$ concentration and in a decline in the MB decolorization [51–53].

3.6. Kinetics study

To better understand the mechanisms in the heterogeneous Fenton reaction, the kinetics during the degradation process needs to be elucidated. In this study, the first-order [Eq. (7)], second-order [Eq. (8)], and Behnajady–
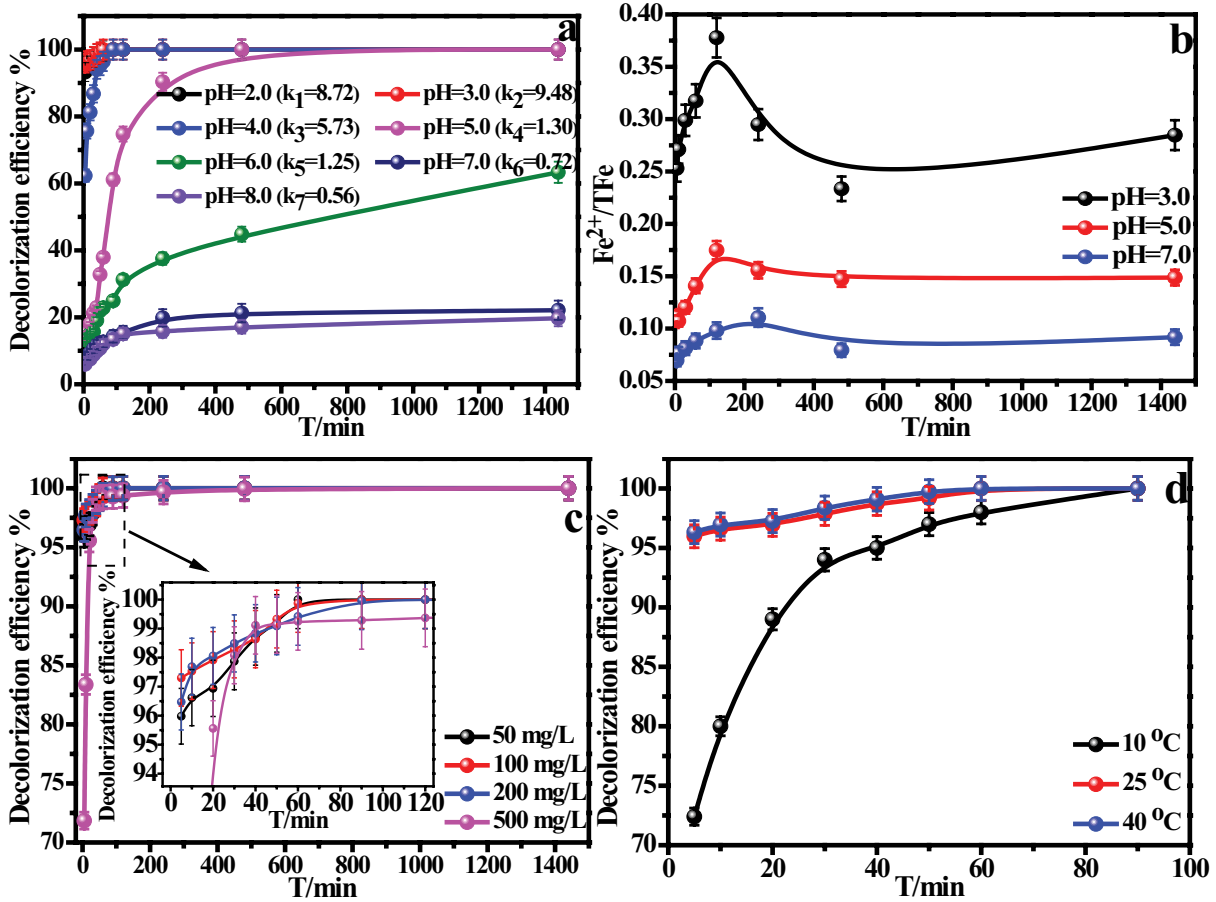
Fig. 3. Effects of (a) initial pH (C_{MB} = 50 mg/L, $C_{H_2O_2}$ = 5.0 mM, ZVI = 69 mg/L, T = 298 K), (b) Fe^{2+}/TFe (ZVI = 69 mg/L, T = 298 K), (c) initial MB concentration (pH = 3.0, $C_{H_2O_2}$ = 5.0 mM, ZVI = 69 mg/L, T = 298 K) and (d) temperature (pH = 3.0, C_{MB} = 50 mg/L, $C_{H_2O_2}$ = 5.0 mM, ZVI = 69 mg/L).

Modirshahla–Ghanbery (BMG) [Eq. (9)] kinetic models [54] were used to analyze the kinetics of the MB degradation at different reaction conditions. The corresponding kinetic formulas are as follows:

$$\ln\left(\frac{C_0}{C_t}\right) = k_1 t \tag{7}$$

$$\frac{1}{C_t} - \frac{1}{C_0} = k_2 t \tag{8}$$

$$\frac{t}{1 - \left(\frac{C_t}{C_0}\right)} = m + bt \tag{9}$$

where C_0 (mg/L) is the initial concentration of MB, C_t (mg/L) represents the MB concentration after the introduction of H_2O_2; k_1 (1/min) and k_2 (mg/L/min) represents the reaction rate coefficient of the first-order and second-order models; m and b are the constants involved in the reaction kinetics and Fenton oxidation capacity limits. The physical meaning of $1/m$ is the initial degradation rate of the substance,

and the higher is the value of $1/m$, the faster is the initial degradation rate of the substance [54]. When the reaction time is sufficiently long to approach infinity, the $1/b$ value represents the theoretical maximum removal efficiency of the material, which is equal to the maximum oxidizing capacity of the Fenton reaction at the end of the reaction [55].

The obtained parameters are shown in Table S1, the values of correlation coefficients of the BMG model are higher than those of the first-order and second-order models. Therefore, the BMG kinetic model is the best model to describe the MB degradation at different reaction conditions.

The effects of the initial pH value, ZVI dose, and the H_2O_2 concentration on the $1/m$ and $1/b$ values are shown in Figs. 5a–c. It can be seen that the $1/m$ value first increases and then decreases with an increase in the initial pH values, ZVI doses, and H_2O_2 concentration, which means that the initial MB degradation rate first increases and then decreases with an increase in the initial pH value, ZVI dose, and H_2O_2 concentration. For $1/b$, the initial MB degradation rate first increases and then decreases with an increase in the initial pH values and H_2O_2 concentration. It can be seen that the theoretical maximum oxidation capacity of ZVI first increases then decreases with an increase in the initial pH values and H_2O_2 concentration. With respect to the pH
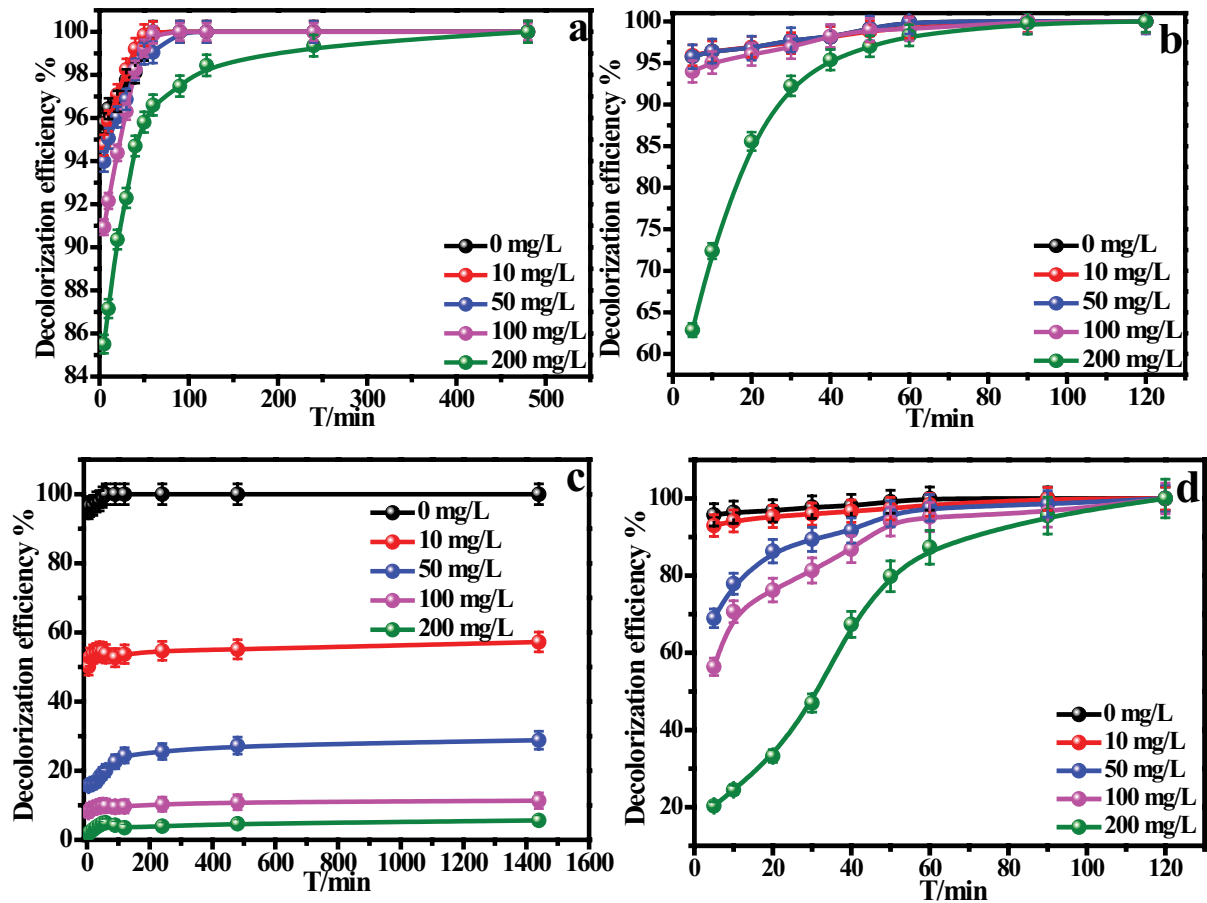
Fig. 4. Effects of (a) different Cl^- concentrations, (b) different SO_4^{2-} concentrations, (c) different NO_2^- concentrations, and (d) different NO_3^- concentrations (pH = 3.0, C_{MB} = 50 mg/L, $C_{H_2O_2}$ = 5.0 mM, T = 298 K).
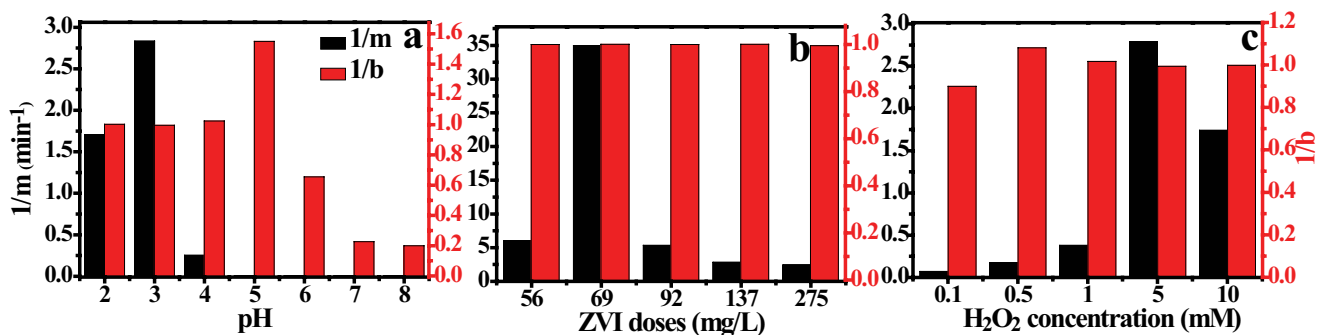
Fig. 5. Effect of different conditions on the values of $1/m$ and $1/b$.

(Fig. 5a), the value of $1/b$ at the pH value range from 5.0 to 8.0 sharply decreases. This occurs because the higher solution pH is not conducive to the production of HO· due to the reduction of dissolved Fe^{2+}. Fig. 5b shows that when the ZVI doses increase, the $1/b$ value remains at approximately 1, which indicates that the maximum oxidizing capacity of ZVI achieved balance at a specific dose. Meanwhile, for the H_2O_2 concentration in Fig. 5c, the maximum oxidizing capacity of the catalyst reaches a maximum when the concentration of H_2O_2 reaches 0.5 mM, and then, the maximum

oxidizing capacity decreases. This phenomenon occurs because excess H_2O_2 reacts with $HO^{\bullet}$ to form other free radicals for which the oxidizing capacity is weaker than that of $HO^{\bullet}$ [56].

3.7. Reusability

To explore the stability of ZVI in practical applications, a cycling experiment was conducted at pH = 3.0, 50 mg/L MB, 5.0 mM H_2O_2, and 69 mg/L ZVI by reusing ZVI seven

times to study the MB decolorization. After every 8 h of reaction, the solution was centrifuged, and a reusable ZVI was obtained for the next experiment.

Fig. 6a shows that 94% MB decolorization efficiency was achieved for seven cycles. Therefore, ZVI has a recyclability potential for the dye wastewater treatment process, and it also has good economic benefits for experimental applications. Fig. 6b shows the mineralization capacity of ZVI in a different system. When only ZVI or H_2O_2 was added, the TOC removal was very bad. However, in the presence of ZVI and H_2O_2, the TOC removal efficiency at pH = 3.0 was higher than that at pH = 5.0, 7.0, and 8.0, which is consistent with the previous experimental results in Figs. 2a and b, and 3a. Less than 50% TOC of the MB solution was degraded with a high removal rate (nearly 100%), which indicates that MB was converted into colorless intermediates. It was reported that the intermediates of the MB degradation mainly include benzoquinone, hydroquinone, catechol, and resorcinol. The aromatic ring intermediate is further oxidized by HO• into short-chain carboxylic acids such as oxalic acid, formic acid, and fumaric acid [57,58].

4. Mechanism exploration

In the heterogeneous Fenton reaction, HO• is essential for removing the active group [59]. Radical capture experiments were carried out by the addition of p-benzoquinone (BQ, 1.0 mM) and *tert*-butanol (TBA, 100.0 mM) to identify reactive species. HO• is effectively captured by *tert*-butanol, while $HO_2^•$ is quenched by BQ [60]. Fig. 7a shows that the decolorization efficiency of MB reduced from 100% to 30% after the addition of *tert*-butanol, which implies that HO•, which is produced by the heterogeneous Fenton-like process, is essential for the MB degradation. When BQ was added, the MB decolorization remained almost unchanged, which indicated that $HO_2^•$ was not involved in the MB degradation.

To detect the generation of HO•, an EPR experiment was carried out during the catalytic reaction process. After 5 min of catalytic degradation, DMPO was selected as a spin trapping agent to capture HO•. Fig. 7b shows that the characteristic peaks of DMPO-OH adducts with an intensity ratio of 1:2:2:1 are obtained in the ZVI/H_2O_2 system,
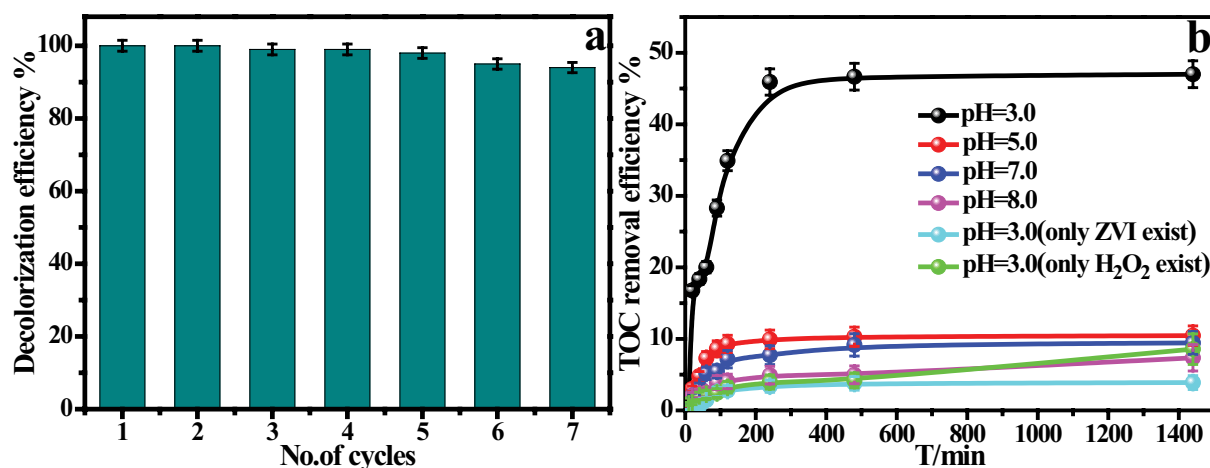
Fig. 6. (a) Reusability of ZVI and (b) the TOC removal efficiency (pH = 3.0, C_{MB} = 50 mg/L, $C_{H_2O_2}$ = 5.0 mM, T = 298 K).
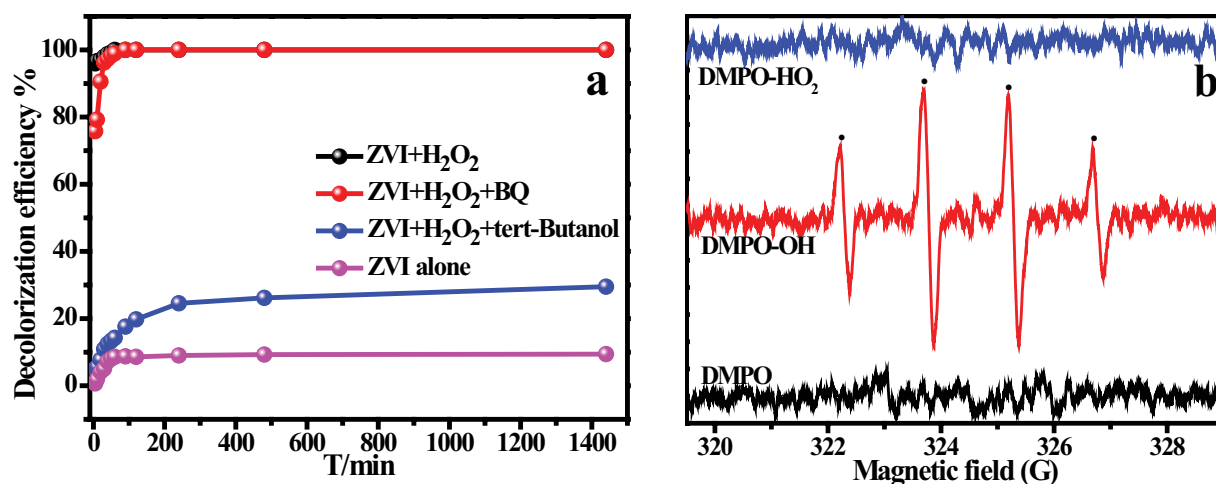
Fig. 7. (a) Effect of radical scavengers on the degradation of MB. EPR spectra of DMPO-OH and (b) DMPO-OOH adduct signals in the ZVI/H_2O_2 system (pH = 3.0, $C_{H_2O_2}$ = 5.0 mM, T = 298 K).

while the characteristic peaks of the DMPO-HO$_2$ adducts with an intensity ratio of 1:1:1:1 were not observed, which is consistent with the results in Fig. 7a.

5. Conclusions

In this study, ZVI was prepared by the thermal treatment of hematite in a hydrogen atmosphere. The XRD results showed that oolitic hematite was gradually converted into magnetite and then completely reduced to ZVI with an increase in the activation temperature from 300°C to 600°C. It was determined that ZVI/H$_2$O$_2$ system can effectively degrade MB solution at pH = 3.0, 5.0 mM H$_2$O$_2$, and 69 mg/L ZVI, and the BMG kinetic model could describe the MB degradation process well. It was shown that the initial degradation rate first increased and then decreased with an increase in the initial pH values, ZVI doses, and H$_2$O$_2$ concentration. ZVI exhibits high performance and reusability during seven cycles. Furthermore, the TOC results showed that MB can be mineralized only in the ZVI/H$_2$O$_2$ system. Though the mineralization of MB was incomplete, the decolorization was pronounced. In addition, from the EPR analysis and the inhibition of TBA and BQ, HO$^\bullet$ rather than HO$_2^\bullet$ was generated by ZVI and catalyzed H$_2$O$_2$, which was essential for the MB decolorization in the ZVI/H$_2$O$_2$ system. In summary, ZVI, which was produced by the calcination of oolitic hematite with H$_2$, has considerable potential in the treatment of dye water. In addition, the study provides a new approach for the comprehensive utilization of naturally occurring hematite.

Acknowledgments

References

[1]	A. Asghar, A.A. Abdul Raman, W.M.A. Wan Daud, Advanced oxidation processes for *in-situ* production of hydrogen peroxide/hydroxyl radical for textile wastewater treatment: a review, J. Cleaner Prod., 87 (2015) 826–838.
[2]	E. Neyens, J. Baeyens, A review of classic Fenton's peroxidation as an advanced oxidation technique, J. Hazard. Mater., 98 (2003) 33–50.
[3]	Y. Gao, Y. Wang, H. Zhang, Removal of Rhodamine B with Fe-supported bentonite as heterogeneous photo-Fenton catalyst under visible irradiation, Appl. Catal., B, 178 (2015) 29–36.
[4]	F. Gosselin, L.M. Madeira, T. Juhna, J.C. Block, Drinking water and biofilm disinfection by Fenton-like reaction, Water Res., 47 (2013) 5631–5638.
[5]	Q. Guo, W. Zi, F. Fei, F. Yue, L. Hai, X. Hui, Fenton-like degradation of Methylene blue using paper mill sludge-derived magnetically separable heterogeneous catalyst: characterization and mechanism, J. Environ. Sci., 35 (2015) 20–26.
[6]	A. Nezamzadeh-Ejhieh, M. Karimi-Shamsabadi, Comparison of photocatalytic efficiency of supported CuO onto micro and nano particles of zeolite X in photodecolorization of Methylene blue and Methyl orange aqueous mixture, Appl. Catal., A, 477 (2014) 83–92.
[7]	X. Liu, S. Chao, L. Chen, Y. Hua, M. Zhu, Y. Bai, S. Feng, S.T. Yang, Decoloration of methylene blue by heterogeneous Fenton-like oxidation on Fe$_3$O$_4$/SiO$_2$/C nanospheres in neutral environment, Mater. Chem. Phys., 213 (2018) 231–238.
[8]	F. Sun, H. Liu, H. Wang, D. Shu, T. Chen, X. Zou, F. Huang, D. Chen, A novel discovery of a heterogeneous Fenton-like system based on natural siderite: a wide range of pH values from 3 to 9, Sci. Total Environ., 698 (2020) 134293.
[9]	N.N. Tusar, D. Maucec, M. Rangus, I. Arcon, M. Mazaj, M. Cotman, A. Pintar, V. Kaucic, Manganese functionalized silicate nanoparticles as a Fenton-type catalyst for water purification by advanced oxidation processes (AOP), Adv. Funct. Mater., 22 (2012) 820–826.
[10]	D.H. Bremner, A.E. Burgess, D. Houllemare, K.C. Namkung, Phenol degradation using hydroxyl radicals generated from zero-valent iron and hydrogen peroxide, Appl. Catal., B, 63 (2006) 15–19.
[11]	M. Chang, H. Shu, H. Yu, An integrated technique using zero-valent iron and UV/H$_2$O$_2$ sequential process for complete decolorization and mineralization of C.I. Acid Black 24 wastewater, J. Hazard. Mater., 138 (2006) 574–581.
[12]	N. Ertugay, F.N. Acar, Sonocatalytic degradation of Direct Blue 71 azo dye at the presence zero-valent iron (ZVI), Desal. Water Treat., 51 (2013) 7570–7576.
[13]	X. Xue, K. Hanna, M. Abdelmoula, N. Deng, Adsorption and oxidation of PCP on the surface of magnetite: kinetic experiments and spectroscopic investigations, Appl. Catal., B, 89 (2009) 432–440.
[14]	K. Zhao, H. Guo, X. Zhou, Adsorption and heterogeneous oxidation of arsenite on modified granular natural siderite: characterization and behaviors, Appl. Geochem., 48 (2014) 184–192.
[15]	Z. Lin, X. Ma, L. Zhao, Y. Dong, Kinetics and products of PCB28 degradation through a goethite-catalyzed Fenton-like reaction, Chemosphere, 101 (2014) 15–20.
[16]	L. Zhou, T.L. Thanh, J. Gong, J.H. Kim, E.J. Kim, Y. Chang, Carboxymethyl cellulose coating decreases toxicity and oxidizing capacity of nanoscale zerovalent iron, Chemosphere, 104 (2014) 155–161.
[17]	H.I. Gomes, C. Dias-Ferreira, L.M. Ottosen, A.B. Ribeiro, Electrodialytic remediation of polychlorinated biphenyls contaminated soil with iron nanoparticles and two different surfactants, J. Colloid Interface Sci., 433 (2014) 189–195.
[18]	G. Xu, J. Wang, M. Lu, Complete debromination of decabromodiphenyl ether using the integration of *Dehalococcoides* sp. strain CBDB1 and zero-valent iron, Chemosphere, 117 (2014) 455–461.
[19]	H. Ma, Y. Huang, M. Shen, D. Hu, H. Yang, M. Zhu, S. Yang, X. Shi, Enhanced decoloration efficacy of electrospun polymer nanofibers immobilized with Fe/Ni bimetallic nanoparticles, RSC Adv., 3 (2013) 6455–6465.
[20]	X. Qiu, Z. Fang, X. Yan, W. Cheng, K. Lin, Chemical stability and toxicity of nanoscale zero-valent iron in the remediation of chromium-contaminated watershed, Chem. Eng. J., 220 (2013) 61–66.
[21]	F. Fu, D.D. Dionysiou, H. Liu, The use of zero-valent iron for groundwater remediation and wastewater treatment: a review, J. Hazard. Mater., 267 (2014) 194–205.
[22]	J.A. Donadelli, L. Carlos, A. Arques, F.S.G. Einschlag, Kinetic and mechanistic analysis of azo dyes decolorization by ZVI-assisted Fenton systems: pH-dependent shift in the contributions of reductive and oxidative transformation pathways, Appl. Catal., B, 231 (2018) 51–61.
[23]	V. Bokare, K. Murugesan, Y.M. Kim, J.R. Jeon, E.J. Kim, Y. Chang, Degradation of triclosan by an integrated nano-bio redox process, Bioresour. Technol., 101 (2010) 6354–6360.
[24]	M. Bystrzejewski, Synthesis of carbon-encapsulated iron nanoparticles via solid state reduction of iron oxide nanoparticles, J. Solid State Chem., 184 (2011) 1492–1498.
[25]	R. Cheng, C. Cheng, G. Liu, X. Zheng, G. Li, J. Li, Removing pentachlorophenol from water using a nanoscale zero-valent iron/H$_2$O$_2$ system, Chemosphere, 141 (2015) 138–143.
[26]	H. Wang, T. Chen, D. Chen, X. Zou, M. Li, F. Huang, F. Sun, C. Wang, Sulfurized oolitic hematite as a heterogeneous

Fenton-like catalyst for tetracycline antibiotic degradation, Appl. Catal., B, 260 (2020) 118203.

[27] J. Zhang, L. Hu, Y. Liang, H. Yang, D. Sun, The research on refractory oolitic hematite and expectation, China Mining Ind., 16 (2007) 74–76.

[28] H. Guo, D. Stüben, Z. Berner, Removal of arsenic from aqueous solution by natural siderite and hematite, Appl. Geochem., 22 (2007) 1039–1051.

[29] H. Guo, D. Stuben, Z. Berner, U. Kramar, Adsorption of arsenic species from water using activated siderite-hematite column filters, J. Hazard. Mater., 151 (2008) 628–635.

[30] Y. Zhang, H. Liu, D. Chen, T. Chen, The application of modified hematite for removal of carmine red dye: performance and mechanism, Desal. Water Treat., 153 (2019) 300–311.

[31] Y. Zhao, R. Zhang, H. Liu, M. Li, T. Chen, D. Chen, X. Zou, R.L. Frost, Green preparation of magnetic biochar for the effective accumulation of Pb(II): performance and mechanism, Chem. Eng. J., 375 (2019) 122011.

[32] H. Wang, T. Chen, H. Liu, W. Li, X. Zou, C. Wang, M. Li, Comprehensive application of oolitic hematite for H_2S removal at high temperature: performance and mechanism, Energy Fuels, 33 (2019) 2037–2044.

[33] Y. Xi, Z. Sun, T. Hreid, G.A. Ayoko, R.L. Frost, Bisphenol A degradation enhanced by air bubbles via advanced oxidation using in situ generated ferrous ions from nano zero-valent iron/palygorskite composite materials, Chem. Eng. J., 247 (2014) 66–74.

[34] S. Hu, H. Yao, K. Wang, C. Lu, Y. Wu, Intensify removal of nitrobenzene from aqueous solution using nano-zero valent iron/granular activated carbon composite as Fenton-like catalyst, Water Air Soil Pollut., 226 (2015) 155–167.

[35] S. Zha, Y. Cheng, Y. Gao, Z. Chen, M. Megharaj, R. Naidu, Nanoscale zero-valent iron as a catalyst for heterogeneous Fenton oxidation of amoxicillin, Chem. Eng. J., 255 (2014) 141–148.

[36] S. Rahim Pouran, A.A. Abdul Raman, W.M.A. Wan Daud, Review on the application of modified iron oxides as heterogeneous catalysts in Fenton reactions, J. Cleaner Prod., 64 (2014) 24–35.

[37] Y. Wu, L.F, S. Hu, S. Wang, H. Yao, K. Wang, Role of dissolved iron ions in nanoparticulate zero-valent iron/H_2O_2 Fenton-like system, Int. J. Environ. Sci. Technol., 16 (2019) 4551–4562.

[38] R. Idel-aouad, M. Valiente, A. Yaacoubi, B. Tanouti, M. Lopez-Mesas, Rapid decolourization and mineralization of the azo dye C.I. Acid Red 14 by heterogeneous Fenton reaction, J. Hazard. Mater., 186 (2011) 745–750.

[39] A.E.H. Machado, J.A.D. Miranda, R.F.D. Freitas, E.T.F.M. Duarte, L.F. Ferreira, Y.D.T. Albuquerque, R. Ruggiero, C. Sattler, L.D. Oliveira, Destruction of the organic matter present in effluent from a cellulose and paper industry using photocatalysis, J. Photochem. Photobiol., A, 155 (2003) 231–241.

[40] J. Kochany, A. Lugowski, Application of Fenton's reagent and activated carbon for removal of nitrification inhibitors, Environ. Technol., 19 (2010) 425–429.

[41] M. Pera-Titus, V. García-Molina, M.A. Baños, J. Giménez, S. Esplugas, Degradation of chlorophenols by means of advanced oxidation processes: a general review, Appl. Catal., B, 47 (2004) 219–256.

[42] Y. Wang, Y. Gao, L. Chen, H. Zhang, Goethite as an efficient heterogeneous Fenton catalyst for the degradation of methyl orange, Catal. Today, 252 (2015) 107–112.

[43] S. Zhang, D. Wang, L. Zhou, X. Zhang, P. Fan, X. Quan, Intensified internal electrolysis for degradation of methylene blue as model compound induced by a novel hybrid material:

[44] J. Feng, X. Hu, P. Yue, Effect of initial solution pH on the degradation of Orange II using clay-based Fe nanocomposites as heterogeneous photo-Fenton catalyst, Water Res., 40 (2006) 641–646.

[45] Y. Kang, K.Y. Hwang, Effects of reaction conditions on the oxidation efficiency in the Fenton process, Water Res., 34 (2000) 2786–2790.

[46] Y. Zhang, T. Chen, Y. Zhao, D. Chen, Y. Zhou, H. Liu, Catalytic effect of siderite on H_2O_2 oxidation of carmine dye: performance, mechanism and kinetics, Appl. Geochem., 106 (2019) 26–33.

[47] H. Gallard, J. De Laat, B. Legube, Spectrophotometric study of the formation of iron(III)-hydroperoxy complexes in homogeneous aqueous solutions, Water Res., 33 (1999) 2929–2936.

[48] Y. Liu, A. Zhou, Y. Gan, X. Li, Effects of inorganic anions on carbon isotope fractionation during Fenton-like degradation of trichloroethene, J. Hazard. Mater., 308 (2016) 187–191.

[49] W. Luo, L. Zhu, N. Wang, H. Tang, M. Cao, Y. She, Efficient removal of organic pollutants with magnetic nanoscaled $BiFeO_3$ as a reusable heterogeneous Fenton-like catalyst, Environ. Sci. Technol., 44 (2010) 1786–1791.

[50] X. Meng, S. Yan, W. Wu, G. Zheng, L. Zhou, Heterogeneous Fenton-like degradation of phenanthrene catalyzed by schwertmannite biosynthesized using *Acidithiobacillus ferrooxidans*, RSC Adv., 7 (2017) 21638–21648.

[51] J.J. López Peñalver, C.V. Gómez Pacheco, M. Sánchez Polo, J. Rivera Utrilla, Degradation of tetracyclines in different water matrices by advanced oxidation/reduction processes based on gamma radiation, J. Chem. Technol. Biotechnol., 88 (2013) 1096–1108.

[52] J. Wang, R. Zhuan, L. Chu, The occurrence, distribution and degradation of antibiotics by ionizing radiation: an overview, Sci. Total Environ., 646 (2019) 1385–1397.

[53] W. Wang, J. Song, X. Han, Schwertmannite as a new Fenton-like catalyst in the oxidation of phenol by H_2O_2, J. Hazard. Mater., 262 (2013) 412–419.

[54] M.A. Behnajady, N. Modirshahla, F. Ghanbary, A kinetic model for the decolorization of C.I. Acid Yellow 23 by Fenton process, J. Hazard. Mater., 148 (2007) 98–102.

[55] H. Xu, T. Shi, L. Wu, S. Qi, Discoloration of Methyl Orange in the presence of schorl and H_2O_2: kinetics and mechanism, Water Air Soil Pollut., 224 (2013) 1740–1750.

[56] B. Sun, H. Li, X. Li, X. Liu, C. Zhang, H. Xu, X. Zhao, Degradation of organic dyes over Fenton-like Cu_2O–Cu/C catalysts, Ind. Eng. Chem. Res., 57 (2018) 14011–14021.

[57] F. Huang, L. Chen, H. Wang, Z. Yan, Analysis of the degradation mechanism of methylene blue by atmospheric pressure dielectric barrier discharge plasma, Chem. Eng. J., 162 (2010) 250–256.

[58] M.A. Rauf, M.A. Meetani, A. Khaleel, A. Ahmed, Photocatalytic degradation of Methylene blue using a mixed catalyst and product analysis by LC/MS, Chem. Eng. J., 157 (2010) 373–378.

[59] L. Chen, J. Ma, X. Li, J. Zhang, J. Fang, Y. Guan, P. Xie, Strong enhancement on Fenton oxidation by addition of hydroxylamine to accelerate the ferric and ferrous iron cycles, Environ. Sci. Technol., 45 (2011) 3925–3930.

[60] Y. Lin, D. Li, J. Hu, G. Xiao, J. Wang, W. Li, X. Fu, Highly efficient photocatalytic degradation of organic pollutants by PANI-modified TiO_2 composite, J. Phys. Chem. C, 116 (2012) 5764–5772.

Supplementary information

Table S1
Kinetic parameters of three models and their correlation coefficients at different reaction conditions

Conditions		First-order kinetic		Second-order kinetic		BMG model		
		k_1 (1/min)	R^2	k_2 (mg/L/min)	R^2	$1/m$ (1/min)	$1/b$	R^2
pH	2.0	0.048	0.9873	0.0751	0.7919	1.7047	1.0027	0.9999
	3.0	0.0349	0.9608	0.041	0.8715	2.8337	0.9958	0.9999
	4.0	0.0431	0.9762	0.0101	0.9375	0.2517	1.0245	0.9982
	5.0	0.01	0.9785	0.0008	0.9325	0.0089	1.5499	0.9741
	6.0	0.0006	0.9227	$2e^{-5}$	0.976	0.0063	0.6553	0.9796
	7.0	0.0007	0.9489	$2e^{-5}$	0.9542	0.0064	0.2262	0.9989
	8.0	0.0009	0.971	$2e^{-5}$	0.97	0.0051	0.2	0.998
ZVI dose	275 mg/L	0.0298	0.9482	0.0388	0.8181	2.4219	0.9956	0.99991
	137 mg/L	0.0473	0.9189	0.1463	0.6212	2.8417	1.0011	1
	92 mg/L	0.0588	0.946	0.1598	0.8079	5.3419	1.0001	1
	69 mg/L	0.2085	0.9944	7.2545	0.9474	34.965	1.0013	1
	56 mg/L	0.0451	0.9814	0.2272	0.7741	6.0205	1.0004	1
H_2O_2 concentration	0.1 mM	0.011	0.9862	0.0008	0.9556	0.0703	0.8992	0.9953
	0.5 mM	0.0614	0.9888	0.0226	0.7237	0.1757	1.0804	0.9989
	1 mM	0.0506	0.9191	0.0276	0.6911	0.3789	1.0169	0.9971
	5 mM	0.0321	0.9091	0.0381	0.7547	2.791	0.9936	0.9999
	10 mM	0.036	0.9689	0.0372	0.9027	1.7413	0.9981	0.9999